Annual Report of
ADVENTURE Project
ADV-99-1 (1999)

# PATCH TEST OF HEXAHEDRAL ELEMENT

**Yoshikazu ISHIHARA**[*1] **and Hirohisa NOGUCHI**[*2]

*1 Mitsubishi Research Institute, Inc.
e-mail: y-ishi@mri.co.jp

*2 Department of System Design Engineering
Keio University,
e-mail: noguchi@keio.ac.jp

**Key words:** hexahedral meshes, finite element, geometrical parameter, coarse mesh, enhanced assumed strain method, quality test

**Abstract**

Generations of hexahedral meshes, all of which are in good quality, seems almost impossible and severely distorted finite elements are frequently generated so that the numerical accuracy may be lost. Therefore, in this paper, the quality of generated hexahedral meshes is firstly investigated by using several geometrical parameters, which affect the accuracy of linear analyses. The enhanced assumed strain (EAS) method, which originally proposed by Simo et al., possesses good coarse mesh and distortion insensitivity properties. Then the accuracy of the EAS elements are is secondly examined through the proposed quality tests in comparison to the displacement based finite elements. The quality of meshes is evaluated by comparing with the theoretical or convergent solution and by checking stress jumps at element boundaries. Finally most critical geometrical parameters for generating hexahedral meshes as well as the accuracy of the EAS elements are clarified statistically by the proposed quality tests.

## 1 INTRODUCTION

In the last decades, a number of automatic mesh generators for finite elements have been proposed so far. However, generation of hexahedral meshes, all of which are in good quality, seems almost impossible and severely distorted finite elements are frequently generated so that the numerical accuracy may be lost. Therefore, in this paper, the quality of generated hexahedral meshes is firstly investigated by using several geometrical parameters, which affect the accuracy of linear analyses.

On the other hand, it is known that low-order continuum finite elements exhibit poor performance or lock in bending or nearly incompressible state and considerable attention has been denoted to the development of low-order elements that exhibit high accuracy in even coarse meshes. The enhanced assumed strain (EAS) method, which originally proposed by Simo et al., possesses good coarse mesh and distortion insensitivity properties. Then the accuracy of the EAS elements are is secondly examined through the proposed quality tests in comparison to the displacement based finite elements.

In the quality tests, hexahedral meshes are generated according to the value of new three-dimensional distortion parameter in several benchmark problems including bending or nearly incompressible state. The quality of meshes is evaluated by comparing with the theoretical or convergent solution and by checking stress jumps at element boundaries. Finally most critical geometrical parameters for generating hexahedral meshes as well as the accuracy of the EAS elements are clarified statistically by the proposed quality tests.

The outline of this paper is as follows. In section 2 the finite element formulations of the EAS method are briefly reviewed and in section 3 the parameters to estimate element distortion are defined. In section 5 numerical examples are presented.

## 2 ENHANCED ASSUMED STRAIN METHOD

The variational basis of EAS method is well-known three-field Hu-Washizu principle. For linear elasticity, it can be written as

$$\Pi(\boldsymbol{u},\boldsymbol{\varepsilon},\boldsymbol{\sigma}) = \int_{\Omega_e} \frac{1}{2}(\boldsymbol{\varepsilon}^T \boldsymbol{C}\,\boldsymbol{\varepsilon} - \boldsymbol{\sigma}^T\boldsymbol{\varepsilon} + \boldsymbol{\sigma}^T\nabla\,\boldsymbol{u})d\Omega - W_e(\boldsymbol{u}) \tag{1}$$

where $\boldsymbol{u},\boldsymbol{\varepsilon},\boldsymbol{\sigma}$ represent displacement, strains and stresses, respectively. **C** stands for the stress-strain matrix, $\nabla$ for the differential operator, and $\Omega_e$ is the element domain. Keypoint of the EAS method is the strain approximation

$$\boldsymbol{\varepsilon} = \nabla\,\boldsymbol{u} + \tilde{\boldsymbol{\varepsilon}} \tag{2}$$

which means that compatible strain field are enhanced by incompatible strain field. Here enhanced strain fields are chosen in a way that they are orthogonal to the stress field.

$$\int_{\Omega_e} \boldsymbol{\sigma}^T \tilde{\boldsymbol{\varepsilon}}\, d\Omega = 0 \tag{3}$$

Substituting eqn (2), (3) into eqn (1), the stress field is eliminated from eqn (1), as a consequence, the final form for the internal energy can be obtained as follows:

$$\Pi(\boldsymbol{u},\tilde{\boldsymbol{\varepsilon}}) = \int_{\Omega_e} \frac{1}{2}(\nabla\,\boldsymbol{u} + \tilde{\boldsymbol{\varepsilon}})^T\,\boldsymbol{D}(\nabla\,\boldsymbol{u} + \tilde{\boldsymbol{\varepsilon}})d\Omega - W_e(\boldsymbol{u}) \tag{4}$$

### 2.1 Finite element interpolations

Continuos displacement and enhanced strain fields are assumed as

$$\boldsymbol{u} = N\,\boldsymbol{d} \tag{5}$$

$$\tilde{\boldsymbol{\varepsilon}} = \boldsymbol{G}\,\boldsymbol{\alpha} \tag{6}$$

**N** is the matrix with the isoparametric shape functions and the **d** the vector of element nodal displacements. **G** is the interpolation matrix and $\alpha$ the vector of internal strain parameters. Substitution of the eqn (5), (6) into the functional of eqn (4) and variation with respect to unknown parameters **d** and $\alpha$ results in the following system of equations:

$$\begin{bmatrix} \boldsymbol{K} & \boldsymbol{L}^T \\ \boldsymbol{L} & \boldsymbol{D} \end{bmatrix} \begin{Bmatrix} \boldsymbol{d} \\ \alpha \end{Bmatrix} = \begin{Bmatrix} \boldsymbol{R} \\ 0 \end{Bmatrix} \tag{7}$$

where

$$\boldsymbol{K} = \int_{\Omega_e} \boldsymbol{B}^T \boldsymbol{C}\boldsymbol{B}\, d\Omega \tag{8}$$

is the usual stiffness matrix of a displacement method and **D** and **L** are defined as

$$\boldsymbol{D} = \int_{\Omega_e} \boldsymbol{G}^T \boldsymbol{C}\,\boldsymbol{G}\, d\Omega \tag{9}$$

$$\boldsymbol{L} = \int_{\Omega_e} \boldsymbol{G}^T \boldsymbol{C}\boldsymbol{B}\, d\Omega \tag{10}$$

Condensation of the strain parameters $\alpha$ yields the element stiffness matrix

$$\boldsymbol{K}' = \boldsymbol{K} - \boldsymbol{L}^T \boldsymbol{D}^{-1} \boldsymbol{L} \tag{11}$$

Which is further processed by the conventional assembly procedure.

## 3 EVALUATION OF DISTORTION

The first page must contain the Title, Author(s), Affiliation(s), Key words and the Abstract. The second page must begin with the Introduction. The first line of the title is located 3cm from the top of the printing box.

### 3.1 Generation of randomly generated meshes

The procedure to generate a mesh is shown in Figure. 1. Uniform and undistorted meshes of size 2 is taken as a basis. Around every node of the undistorted mesh, a bounding sphere of size 2a is defined, where a ( $0 < a < 0.9$ ) a distortion parameter. The node is then moved on the bounding sphere by randomly generated angles $\theta, \varphi$ ( $0 < \theta, \varphi < 2\pi$ ). Geometrical parameters for representing mesh distribution are calculated as follows.

### 3.2 Aspect ratio

Figure 2 shows a definition image of aspect ratio. If the shape of element is cube, the aspect ratio is 1. The more distorted meshes are, the bigger the value of aspect ratio is. In the case of more distorted mesh, the value of aspect ratio becomes bigger.

### 3.3 Angle of normal vector

Angle shows an angle between the normal rectors on the surfaces which face each other. As shown in Figure3, and if the angle is 0 the surfaces are parallel and if it becomes close to larger, the mesh almost is severely distorted.

### 3.4 Flatness

As shown in figure 4, a surface is divided into two triangles and then. Flatness calculated from normal vector ($\mathbf{p}_1$~$\mathbf{p}_4$) at each node point. The average angle between normal vectors at nodes.

## 4 NUMERICAL ANALYSIS AND RESULTS

In the following example, 900 different randomly generated meshes are used for the evaluation of the distorted elements. In the Figure 6, 7, 8, 10, 11 and 12, the average, maximum and minimum values are plotted.

### 4.1 Incompressible bock

A regular incompressible block is considered with side lengths of 100 and a height of 50 (figure. 5). The structure is fixed at the bottom and loaded at the top by a uniform pressure load of q=250/unit area acting on a center area of $20 \times 20$ (Young's module $\mathrm{E} = 2.1 \times 10^5$, Poisson's ratio $\nu = 0.4999$). Figure 5 shows the regular mesh, one of the distorted meshes and the accuracy of analyses results. Figure 6, 7 and 8 show the variation of accuracy with respect to these geometrical parameters. Table 1 shows the correlation coefficient of each geometrical parameters. EAS-30 element avoids volumetric locking and possess higher accuracy than element based on the displacement formulation (DISP). The accuracy of solution is well expressed with geometrical parameters proposed in this paper from Figure 6 to Figure 8. However each geometrical parameters have correlation each other deeply, the most critical parameter can not be determined from this example.

### 4.2 Pinched hemispherical shell

Figure 11 shows one quarter of the hemispherical shell with a free edge pinched by two couples of concentrated loads (Radius $R = 10.0$, thickness $t = 0.04$, Young's module $E = 6.825 \times 10^7$, Poisson's ratio $\nu = 0.3$). Figure 9 shows the regular mesh, one of the distorted meshes and the accuracy of analyses results. Figure 10, 11 and 12 show the variation of accuracy with respect to these geometrical parameters. Table 2 shows the correlation coefficient of the each geometrical parameters. From Figure 9, EAS-30 element possess higher accuracy than DISP, in case of the regular mesh, the accuracy of solution is well expressed with geometrical parameters proposed in this paper, as seen in Figure 10 to Figure 12. In this case, as shown in the Table 2, angles between normals on the surfaces facing each other give great influence to the analyses results.

## 5 CONCLUSION

From the analyses of several problems, this study allows the following conclusions:

(1) The EAS elements are much more robust than the elements based on displacement approximation and those elements exhibit high accuracy in coarse meshes.
(2) In this study, angles of normal vector have most influence on the accuracy among these geometrical parameters.

## REFERENCES

J. C. Simo and M. S. Rifai, A Class of Mixed Assumed Strain Methods and the Method of Incompatible Modes, *Int. j. numer. methods eng.*, **29**, 1990, 1639-1652.

U. Andelfinger and E. Ramm, EAS-Elements for Two-Dimensional, Three-Dimensional, Plate and Shell Structures and Their Equivalence to HR-Elements, *Int. j. numer. methods eng*, **36**, 1993, 1311-1337.

J. Korelc and P. Wriggers, Improved Enhanced Strain Four-Node Element with Taylor Expansion of the Shape Functions, *Int. j. numer. methods eng*., 1997, **40**, 407-421.

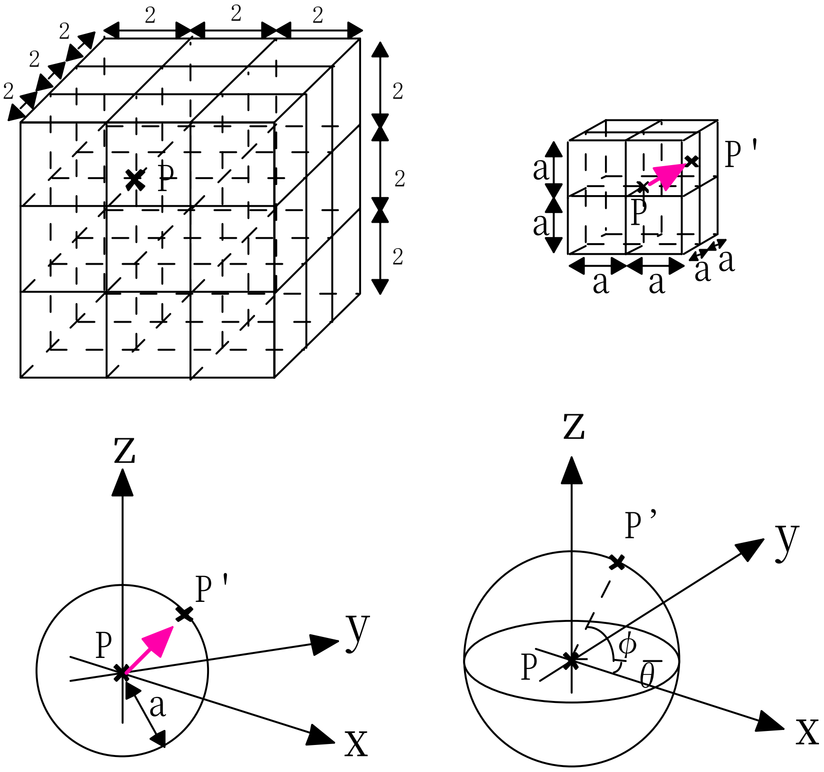


Figure 1 Generation of Randomly Distorted Meshes

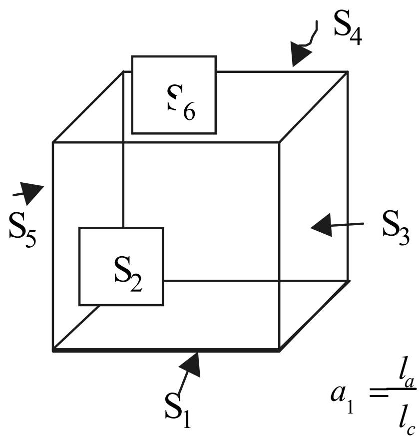


$$l_a = \sqrt{(S_1 + S_6)}$$

$$l_b = \sqrt{(S_2 + S_4)}$$

$$l_c = \sqrt{(S_3 + S_5)}$$

$$l_a \geq l_b \geq l_c$$

$$a_1 = \frac{l_a}{l_c}, \quad a_2 = \frac{l_b}{l_c}, \quad a_1 \geq a_2 \geq 1.0$$

Figure 2 Definition of Aspect Ratio

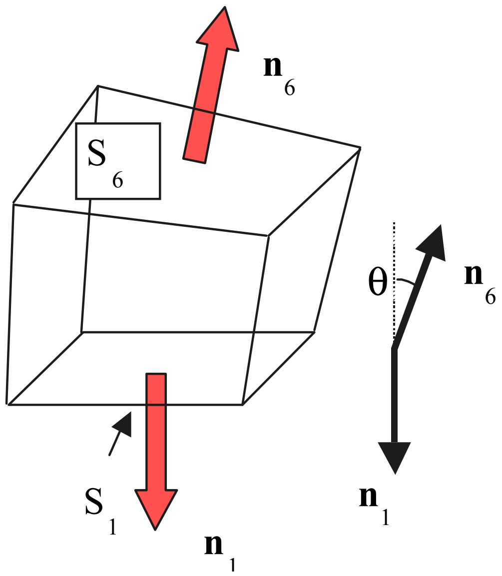


Figure 3 Definition of Angle

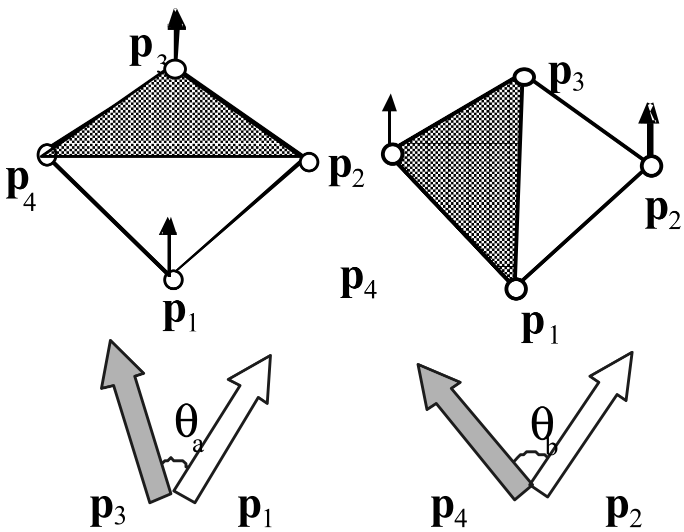


Figure 4 Definition of Flatness

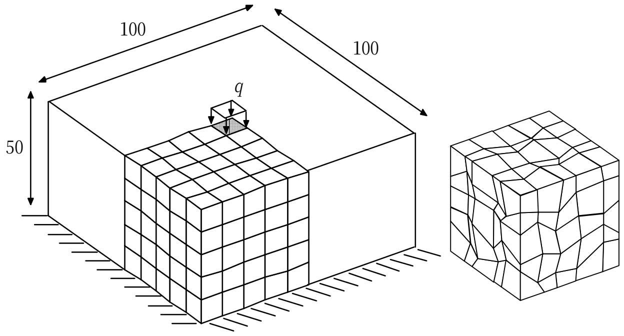


| | *EAS*-30 | *EAS*-21 | *EAS*-9 | *DISP* |
|---|---|---|---|---|
| regular | 0.01905 | 0.01905 | 0.01136 | 0.00160 |
| irregular | 0.01884 | 0.01850 | 0.01194 | 0.00113 |

Figure 5 Model of incompressible block

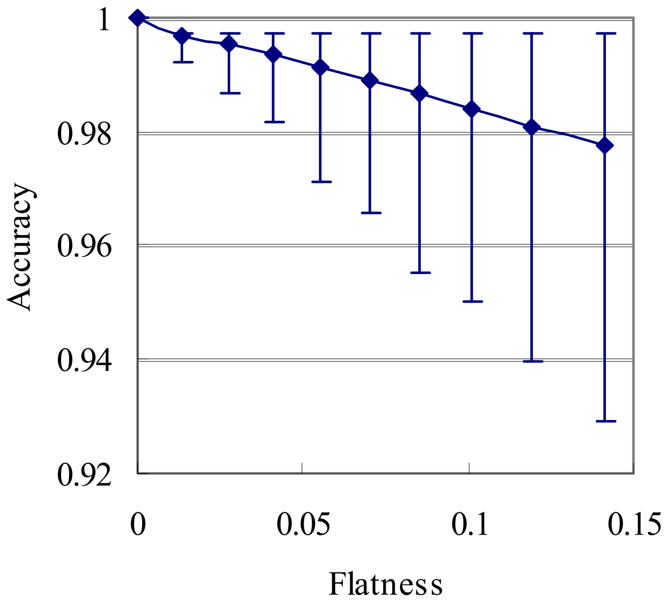


Figure 6 Flatness-accuracy curve (incompressible block)

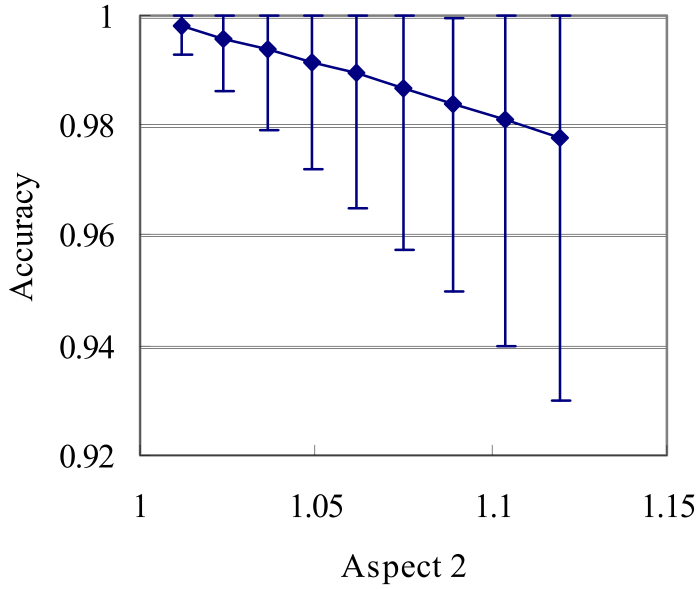


Figure 7 Aspect-accuracy curve (incompressible block)

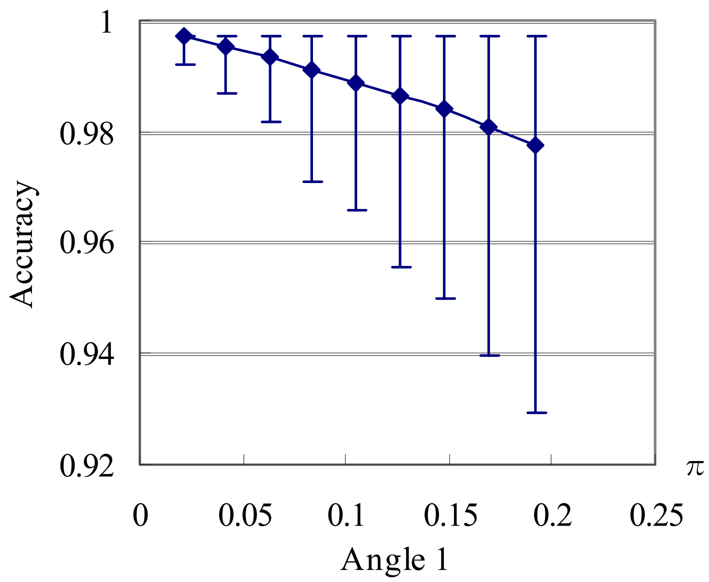


Figure 8 Angle-accuracy curve (incompressible block)

Table 1 CORRELATION COEFFICIENT BETWEEN GEOMETRICAL PARAMETERS
(incompressible block)

| | flatness | aspect 1 | aspect 2 | angle 1 | angle 2 | angle 3 | accuracy |
|---|---|---|---|---|---|---|---|
| flatness | | | | | | | |
| aspect 1 | 0.980 | | | | | | |
| aspect 2 | 0.982 | 0.996 | | | | | |
| angle 1 | 0.987 | 0.988 | 0.989 | | | | |
| angle 2 | 0.993 | 0.986 | 0.992 | 0.994 | | | |
| angle 3 | 0.990 | 0.983 | 0.986 | 0.992 | 0.994 | | |
| accuracy | -0.537 | -0.538 | -0.542 | -0.530 | -0.548 | -0./542 | |

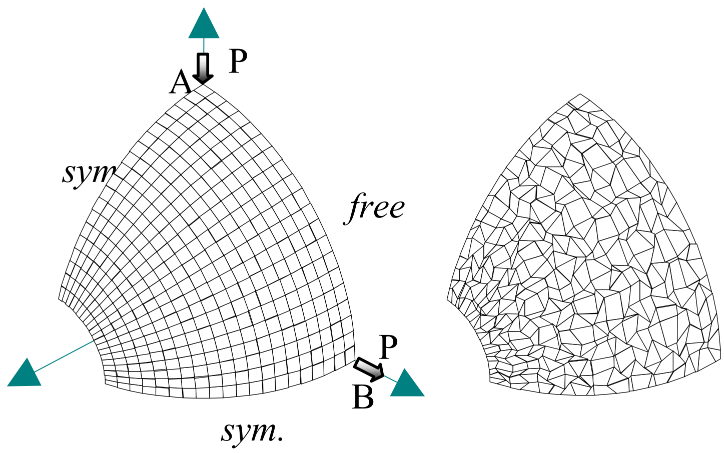


| | *EAS*-30 | *EAS*-21 | *EAS*-15 | *EAS*-9 | *DISP* |
|---|---|---|---|---|---|
| regular | 1.003 | 1.003 | 1.003 | 0.881 | 0.0161 |
| irregular | 0.0878 | 0.0876 | 0.0869 | 0.0490 | 0.0112 |

Figure 9 Model of hemispherical shell

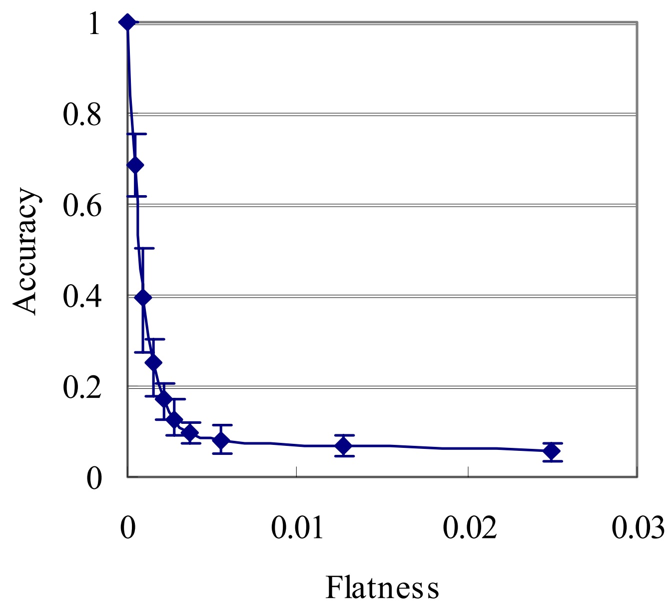


Figure 10 Flatness-accuracy curve (hemispherical shell)

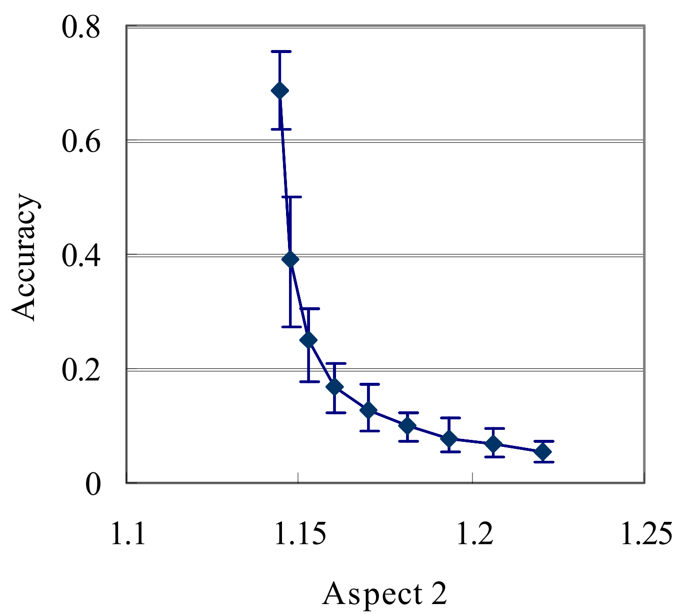


Figure 11 Aspect-accuracy curve(hemispherical shell)

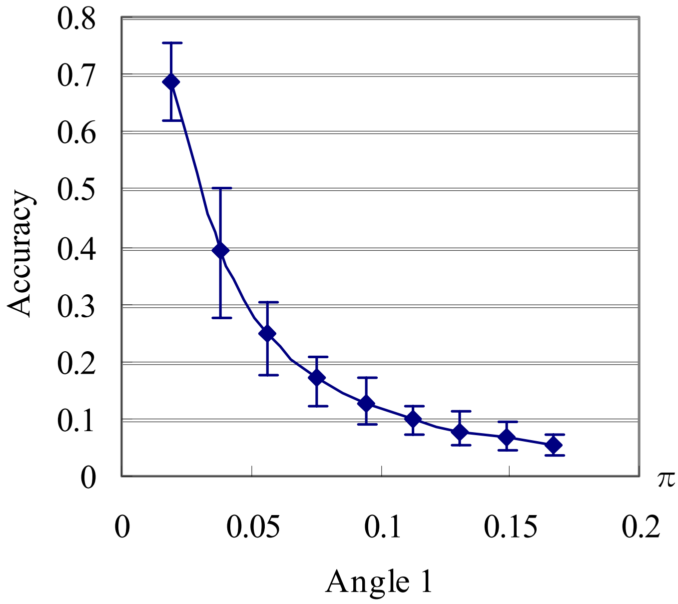


Figure 12 Angle-accuracy curve(hemispherical shell)

Table 2 CORRELATION COEFFICIENT BETWEEN GEOMETRICAL PARAMETERS (hemispherical shell)

| | flatness | aspect 1 | aspect 2 | angle 1 | angle 2 | angle 3 | accuracy |
|---|---|---|---|---|---|---|---|
| flatness | | | | | | | |
| aspect 1 | -0.085 | | | | | | |
| aspect 2 | 0.853 | -0.900 | | | | | |
| angle 1 | 0.798 | -0.944 | 0.945 | | | | |
| angle 2 | 0.823 | -0.954 | 0.952 | 0.989 | | | |
| angle 3 | 0.843 | -0.956 | 0.959 | 0.985 | 0.987 | | |
| accuracy | -0.510 | 0.690 | -0.736 | -0.858 | -0.831 | -0.818 | |